THESIS FOR THE DEGREE OF LICENTIATE OF ENGINEERING

Inconel 718 and Hydrogen

Cathodic charging, mechanical testing and material model description

NIKLAS EHRLIN

Department of Materials and Manufacturing Technology
CHALMERS UNIVERSITY OF TECHNOLOGY
Gothenburg, Sweden 2016

Inconel 718 and Hydrogen
Cathodic charging, mechanical testing and material model description
Niklas Ehrlin
niklas.ehrlin@mah.se

ISSN 1652-8891
No 106/2016

Department of Materials and Manufacturing Technology
Chalmers University of Technology
SE-412 96 Gothenburg
Sweden
Telephone + 46 (0)31-772 1000

Chalmers Reproservice
Gothenburg, Sweden 2016

Inconel 718 and Hydrogen
Cathodic charging, mechanical testing and material model description
NIKLAS EHRLIN
Department of Materials and Manufacturing Technology
CHALMERS UNIVERSITY OF TECHNOLOGY

Abstract

The nickel based superalloy IN718 is known to be sensitive to hydrogen, causing degradation of its mechanical properties. The degrading mechanism commonly proposed is based on an increased mobility and density of dislocations, caused by the dissolved hydrogen. This results in a decreased yield stress and a premature fracture. A physically based flow stress model based on the dislocation density, which incorporates the effects of an increased hydrogen concentration, is proposed. The model parameters are found using experimental data from uncharged and hydrogen pre-charged IN718 samples.

In order to better understand the influence of hydrogen on plasticity behaviour, a well-defined hydrogen distribution is essential in the specimens. The method of charging cylindrical IN718 specimens with hydrogen using cathodic charging is evaluated. The resulting hydrogen concentration is measured for various radii, and compared with computations. It is shown that the anisotropic diffusion coefficient resulting from electromigration, inherent in the charging method, must be taken into account as it has a major impact on the charging parameters of IN718.

Keywords: IN718, Hydrogen Embrittlement, Cathodic Charging, Flow Stress Model

Faculty of Technology and Society

MALMÖ UNIVERSITY

If you want to achieve peace of mind and happiness, then have faith.
If you want to be a disciple of truth, then search.

- F. W. Nietzsche

Acknowledgments

This work was carried out at the group of Materials Science and Applied Mathematics at the Faculty of Technology and Society, Malmö University in cooperation with Materials and Manufacturing Technology, Chalmers University of Technology.

I wish to thank my supervisors Christina Bjerkén and Martin Fisk for initiating this project and continuously supporting it and my progression. My other bright coworkers in Malmö should of course not be forgotten, with a special thank you to Claudio Nigro for his brilliant coding expertise.

A special thanks also to Lars-Erik Lindgren and Bijsh Babu for the great work on the optimisation platform, which enables our work.

Olof Hultin deserves a thank you for the nice SEM sessions.

And most importantly, a heartfelt thanks to my lovely wife Åsa, our beautiful kids Emmi and Ebba and to our extended family. Thank you all for making our lives fabulous!

The work was carried out with financial support from Malmö Högskola and the Swedish Research Council, grant 621-2012-3698.

Niklas Ehrlin
Malmö, Sweden

September, 2016

Ethics and sustainability considerations

As the project does not involve any human subjects, my main ethics concern would be regarding one of the stakeholders; namely the taxpayers of Sweden. A concern that has been raised lately is why a lot of research results that are funded by tax money, never get fully accessible for the taxpayers. Especially in Sweden which have a high level of public access to official records, it is remarkable that most of the scientific work only can be accessed (if all) via the University libraries. This makes it hard for that group of stakeholders to evaluate if the spent money is used well. It also feels somewhat problematic in an ethic and transparency point of view, why publishing Open Access should be preferred. Even if this is a clear demand from the funder and in many cases also from the University itself, this does not automatically means that publications will be published as Open Access. Furthermore, ensuring Open Access is in my opinion a great step in the direction of reducing the gap between the scientific community and the rest, but it is most likely not enough. The scientific knowledge regarding material behavior is getting more and more detailed. Simulations are seeing an increase in use and are more accurately describing the real physics of materials. This knowledge is not anymore only used by one or a few specialists at a production or foundry-place, but seeing new areas of use such as the gaming industry. Even if the knowledge on material mechanics spreads, it is still limited to a small part of a population and could perhaps not be considered as arguments on social sustainability and development. But it is still a knowledge development. An Open Access policy only, would perhaps not have a direct positive effect on the knowledge regarding material mechanics and hydrogen interactions of the common taxpayer – but it would certainty not have a negative effect.

The research project is not related to anything with a direct environmental impact or deals with anything hazardous. But since the use of the alloy in this study is spread within both the aerospace and the oil/gas industry, these must be viewed as stakeholders of my research, although not directly involved. And it is fair to assume that any change in the activities within these industries will have consequences on the environment, either positive or negative. An optimistic view would be that improved modeling and simulation capabilities on the material behavior, could help prolonging the life-time of any part manufactured by the alloy. These special alloys demand a highly specialised manufacturing process, with many energy-consuming steps. Furthermore, mining Ni (which is the main metal in the alloy) is connected to a high risk of any eco-systems in the vicinity of the mining area, why a prolonged life-time could reduce the demand for the alloy and hence reduce the environmental impact. A more negative and critical view would use basically the same argument; a prolonged life could very well result in a higher demand for the alloy and hence a higher demand for Ni, and eventually also expand the mentioned industries.

The resulting material model could also help prevent any material failure. And given the type of industries the alloy is used within today, a material failure would have severe consequences on the environment and/or human life.

Even if the resulting material model and simulations are focused on IN718, this could very well be altered and used for other similar materials. One could also envision that the hydrogen energy and hydrogen industry will grow, where any research done on the metal-hydrogen-interactions will be of use.

Appended papers

The work presented in this thesis and its results is prepared for publication as two journal articles and one conference paper. All three are appended at the end of the thesis.

Paper I

Cathodic hydrogen charging of Inconel 718. Niklas Ehrlin, Christina Bjerkén and Martin Fisk. *Submitted to AIMS Materials Science.*

Cathodic hydrogen charging is performed and the method is evaluated with respect to the increased diffusivity of hydrogen ions due to the applied electric field. Charging results are compared to charging simulations and a hydrogen concentration homegenity is concluded. Author's contribution: All literature survey, all experimental work, 90 % of the simulation work and 90% of the writing.

Paper II

Cathodic hydrogen charging of Inconel 718, evaluation and computations. Niklas Ehrlin, Christina Bjerkén and Martin Fisk. *Proceedings of the 2016 International Hydrogen Conference*. Moran, USA. September 2016.

Charging simulations performed for tensile test geometries as well as out-gassing simulations. Author's contribution: All literature survey, all experimental work, 90 % of the simulation work and 90% of the writing.

Paper III

Flow stress model for hydrogen degraded Inconel 718. Niklas Ehrlin, Martin Fisk and Christina Bjerkén. *Manuscript form.*

Tensile tests are performed on hydrogen charged and un-charged IN718 samples. A flow stress model is extended to encompass the effect of hydrogen on the plasticity behaviour, and parameters extracted using an optimisation toolbox. Author's contribution: All literature survey, all experimental work, 70 % of the simulation work and 90% of the writing.

Contents

1 Introduction

Inconel 718, or IN718, is a commercial nickel-chromium-iron based superalloy, which shows thermal and mechanical stability with maintained yield strength and fracture toughness in the temperature range of approx. -250 to 650°C [1]. The alloy has gained much use in gas turbine engines, heat exchange tubing and other high-temperature and high-load applications [2]. The alloy has also found use in environments where high concentrations of hydrogen could be expected, such as natural-gas processing plants and liquid-hydrogen engines [3]. Several studies have been conducted on the hydrogen susceptibility of IN718, and the unanimous conclusion is that IN718 exhibits degradation in properties when subjected to hydrogen [4-6]. The fracture surface morphology of IN718 subjected to hydrogen embrittlement, studied with the use of high resolution electron microscopes [7, 8], gives general observations indicating localised ductile fracture. Based on these observations, Hicks and Altstetter [7] suggested Hydrogen Enhanced Localised Plasticity (HELP) as the mechanism of hydrogen embrittlement in IN718. Other mechanisms generally describing hydrogen embrittlement, *e.g.* hydrogen-induced lattice decohesion or hydride formation would in IN718 require concentration levels of both stress and hydrogen that only, if at all, would be found near a crack-tip.

To study the overall macroscopic effect of the HELP mechanism, hydrogen should preferably be introduced homogeneously into tensile test samples. One way of introducing, or charge samples with hydrogen is to use cathodic hydrogen charging. Even if it is a method that has been used extensively, the literature is sparse in detailed description on the governing parameters when charging participation hardened super alloys. These parameters are needed to quantify the enhanced diffusivity of hydrogen ions because of electromigration in the presence of the applied electric field, which is one of the benefits of the method. A refinement of the charging details is needed in order to keep the charging time at a minimum, or to achieve a specific concentration gradient within the sample.

In this work, the method is used to charge IN718 samples and the concentration homogeneity is measured and compared with computations. Tensile test results on hydrogen charged IN718 samples as well as un-charged samples are used to optimize the parameters of the proposed material model. Any constitutive plasticity model for the HELP mechanism in precipitation hardened alloys has to our knowledge not been presented, which serves as motivation for the work in this thesis. A material model which includes the degrading effect of hydrogen on the mechanical properties would be of great use in order to predict material behavior in hydrogen rich environments.

2 Hydrogen degradation

Hydrogen degradation or hydrogen embrittlement was first reported over a century ago, when the loss of mechanical properties at room temperature of steel and iron containing hydrogen, was noticed. It has since been shown that not only steel and iron are effected by hydrogen, but almost all metals and alloys are susceptible to hydrogen induced premature failure. The embrittlement often manifests as loss of ductility and fracture stress and a change of fracture mode [9]. Internal hydrogen embrittlement is when hydrogen has entered the material before the external load is applied and is usually caused by chemical or electro-chemical preprocessing, solidification of ingots or welding. External, or environmental hydrogen embrittlement, is the term used if the degradation occurs while in a hydrogen environment, where dissociated hydrogen must diffuse from the surface into the material [6]. Many different, often material specific hydrogen-related failure mechanisms has been proposed and subjected to debate, and yet no unified theory has been established [10]. The different theories proposed are often divided into a few areas; internal pressure and hydride embrittlement, hydrogen-induced decohesion and hydrogen enhanced plasticity.

The first area revolves around the increase of internal pressure, caused either by precipitation of molecular hydrogen or by hydride formation [11, 12]. Molecular hydrogen dissociates on the metal surface before entering the metal as atomic hydrogen, with a higher mobility inside the metal. The atomic hydrogen could recombine at voids or interfaces within the material. As molecular hydrogen has a volume greater than the sum of two hydrogen atoms the local hydrostatic stress and internal pressure will increase. Eventually the stress is large enough to rupture the hydrogen-weakened metallic bonds and reduce the overall failure stress [13]. A direct observation of this mechanism in a hydrogen super-saturated iron-3% silicon single crystal has been provided by Tetelman and Robertson [14]. Hydrogen could also form hydrides and hydride-complexes with different metals and alloys which comprises a host lattice and hydrogen atoms. Failure caused by hydride formation has been reported in systems where hydrides either are stable or can be stabilised by a local increase of the stress field. Within the area of superalloys and highly engineered alloys, hydrides are commonly associated with Ti and Zr based alloys [15, 16]. Ni is usually classified as a non-hydride-forming element. However, atomistic simulations have shown that thermodynamically stable local hydrides can form in the Ni-H system. The formation, caused by a considerable strain-induced enhancement of the local hydrogen concentration together with an elevated hydrostatic pressure, may occur even at modest bulk concentrations of hydrogen and ambient conditions [17]. It has further been suggested that the electrochemical process of cathodic charging of hydrogen can promote the formation of so called pseudo-hydrides in the non-hydride-forming metals, such as Ni and its alloys [18]. In the pseudo-hydride phase, hydrogen is only partly solved in the lattice at random interstitial positions, compared to the phase of a fully formed hydride with its ordering of hydrogen in the interstitial positions together with an accompanying change in lattice parameters and volume. Direct observations of this formation due to cathodic charging have also been experimentally observed using X-ray diffraction methods [19, 20].
Closely related is the second mentioned area of hydrogen degradation theories, commonly referred to as *hydrogen-induced decohesion* or *hydrogen-enhanced decohesion*. It is based on

the supersaturation of atomic hydrogen at areas with a high hydrostatic stress (*e.g.* a crack tip) and the interaction where hydrogen weakens the atomic bonds [21]. In this model, the fracture is brittle when the external stress exceeds the *cohesive stress*. Chen *et al.* [22] reports a hydrogen concentration of 5950 at ppm near the crack tip in their experiment using iron-3% silicon single crystals. This concentration was considered as sufficient, with no lower limit concentration reported, to promote lattice decohesion. The decohesion model was further believed to be the dominant degradation effect, opposed to enhanced plasticity effects. This proposed mechanism is dependent on a high hydrogen concentration close to the crack tip, if a crack propagation and failure is to be expected. This requirement can be met either by an environment that results in a supersaturation of hydrogen in the specimen or a very high diffusivity of mobile hydrogen in a pre-charged specimen. Decohesion could also induce cracks in grain boundaries, as the cohesive strength is lowered under the influence of hydrogen. Grain boundary decohesion, just as with crack tip decohesion and lattice decohesion, requires a very high equivalent gas pressure of hydrogen, reportedly 1000 atm and above [23]. Although it is evident that hydrogen does weaken the lattice bond strength and grain boundary cohesive strength, it has been pointed out that the concentration of hydrogen usually is too low to break the bond of the metal atoms and open grain boundaries [23, 24]. Furthermore no direct experimental evidence has been reported supporting lattice decohesion by hydrogen [11].

The last main area of theories regarding hydrogen degradation addresses the effect of hydrogen on dislocations and dislocation kinetics. This topic has been addressed since 1960s regarding either an increase in dislocation generation and/or an alteration of the internal friction and dislocation movement in metals [25-28]. Early experimental reports on the hydrogen-dislocation interactions are commonly based on various tensile tests performed on samples pre-charged with hydrogen. Matsui *et al.* [29, 30] represented an exception with their *in situ* tensile tests on samples in an electrolytic cell. Here, samples of high purity iron, charged with hydrogen during the tensile tests, showed an increase in mobile dislocation density and an alteration of the tensile response. The altered response comprises both softening and hardening, depending on the variation in experimental variables such as current density and strain rate. Both the softening and hardening was, although somewhat speculative, explained by interactions between hydrogen and dislocations.

In 1972, a model of hydrogen-dislocation interactions was proposed by Beachem [31]. He suggested that hydrogen instead of *locking* dislocations, the raised hydrogen concentration lowered the stress needed to move the dislocations and thereby *unlocking* them. Beachem further concludes that if a sufficient concentration of hydrogen is dissolved in the lattice near the crack tip, this will promote a severe local ductile crack-tip deformation. And although this may lead to macroscopic failures that bear the resemblance of a brittle fracture, evidence of the plastic deformation can be seen in the microstructure as dimples and tear ridges. The crack-tip deformation together with the microstructure of the material is believed to cause the sudden low stress fractures and not an overall exhaustion or restriction of ductility. Beachem therefore suggested the term *hydrogen-assisted* cracking rather than *hydrogen embrittlement* cracking [31].

Robertson [9] claims that Beachem's model basically was ignored by the scientific community, until the latter part of the 1970s when the idea of hydrogen-enhanced dislocation mobility, once again surfaced. Close to follow was a direct observation of the enhanced dislocation mobility and local densification [32]. This *in situ* experiment was achieved by the use of an environmental cell with varying pressures of hydrogen gas inside a transmission electron microscope (TEM). In the article, sheets of commercially pure Ni were strained at a low rate at room temperature, within an environment of hydrogen at a pressure of 7 kPa. The authors claim to observe a rapid dislocation movement together with a dislocation multiplication, resulting in a very high local dislocation density.

Birnbaum and co-workers conducted additional *in situ* studies on different metals and alloys, including precipitation strengthened alloys, and almost 20 years after Beachem's model, they presented the phenomena which were named Hydrogen Enhanced Localised Plasticity, or HELP [12, 15, 18, 33].

2.1 Hydrogen-enhanced localised plasticity

The HELP mechanism was proposed as an explanatory model for the decrease in flow stress of metals and alloys in the presence of hydrogen. It differs from the contemporary description of the same phenomena proposed by Lynch [34] by not only being a surface effect, but instead considering the hydrogen effect to occur both near the surface and within the volume of the material. The mechanism is based on the interaction between hydrogen atoms and dislocations with the effect of an increase in dislocation mobility. The increased dislocation motion is explained by a combination of hydrogen diffusion towards the stress field of dislocations and other obstacles, and the shielding, or the lubricating, effect of hydrogen between dislocations and obstacles. Hydrogen thereby modifies this stress field which allows dislocations to locally move at a lower stress relatively to the deforming bulk volume [35]. A reported lower concentration limit for hydrogen to have this effect on the tensile response and observe the HELP mechanism has been suggested to about 50 at ppm [23, 32].

The mechanism is reported not to be dependent on the crystal structure or dislocation type, but mainly dependent on the material purity and hydrogen concentration [23, 35]. The effect is not only supported by extensive *in situ* studies of Birnbaum and co-workers. High resolution fracture studies also support plastic processes as hydrogen softens the material in front of the crack tip, allowing local ductile fracture. According to Birnbaum and Sofronis [15] this is the reason for the observed microscopic ”transgranular” fractures, suggesting that the plastic process does not solely occur along the grain boundaries. And just as Beachem suggested before them, because of the localised nature of the ductile failure, fracture surface examination at low resolution could very well lead to a brittle fracture conclusion.

It has been pointed out that the hypothesised mechanism lacks an unambiguous confirmation from performed mechanical tests [36]. Just as the descriptions prior to HELP, it is most likely not a unifying description of hydrogen induced degradation, but instead a piece of the puzzle.

3 Hydrogen charging

The HELP mechanism describes the interaction between hydrogen and dislocations throughout the material, and is not only a description of surface and/or crack-tip phenomena. To study the effect of hydrogen on the tensile properties of IN718, with a special focus on the HELP mechanism, hydrogen preferably should be introduced into the bulk of tensile test specimens.

Different methods of charging samples with hydrogen have been developed. Gas pressure and autoclave methods rely foremost on a constant high pressure of hydrogen gas around the sample to be charged. For the autoclave method, this is supplemented with an elevated temperature to decrease the charging time, and must be performed in a strictly controlled facility because of the risk of explosion. Hydrogen charging, results in a hydrogen concentration profile, which can be described by the solution of Fick's second law. For a given material and the above mentioned methods, the concentration profile can be altered by varying the parameters of time, temperature and surface concentration of hydrogen. To achieve hydrogen concentration homogeneity in tensile test size samples of IN718, a long holding time or a high pressure of hydrogen together with a high temperature would be required. To instead use the method of cathodic hydrogen charging, is one way of reducing the charging time and the need for high temperature.

3.1 Cathodic hydrogen charging

Cathodic hydrogen charging is a method based on an electrochemical cell, in which the sample acts as the cathode and usually a piece of platinum acts as the anode, both submerged in an electrolyte. Figure. 1 illustrates a typical cathodic charging setup. When an electrical potential is applied across the electrodes, the electrolytic solution decomposes and hydrogen ions (protons) are produced. The applied potential causes a flux in charge carriers, both in the electrolytic solution and in the electrodes. This flux generates a high concentration of hydrogen ions on the surface of the sample. At the same time, the applied potential acts as a complementary driving force for diffusion of the hydrogen ions [37]. In addition to being a less volatile charging method, cathodic charging is claimed to give a faster buildup of hydrogen and results in a higher, more homogeneous concentration in the metal than normally achieved using gas based charging [38]. Varying the charging parameters temperature, current density and time could alter the charging outcome, but this is ultimately limited by the saturation of available atomic hydrogen at the sample surface. However, the main variable among the various charging experiments found in the literature is the electrolytic medium. These electrolytes can be diluted solutions, such as H_2SO_4 in H_2O [39] or methanolic solutions with H_2SO_4 and NaOH, usually together with additions of hydrogen recombination inhibitor ($NaAsO_2$, AsO_3) and hydrogen adsorption promoter (H_2SeO_3) [40-42]. Charging using aqueous or methanolic solutions must be performed below the boiling temperature of the selected solvent. Undiluted electrolytes are *e.g.* molten salts, which usually have a 1:1 molar ratio of $NaHSO_4$ and $KHSO_4$ [3, 38, 43], or NaOH and KOH in the same ratio [7]. The molten salt electrolytes require a minimum temperature of around 200-250°C for the sulphate salts and around 300-350°C for

the hydroxide salts, in order to melt and fuse. The sulphate salt mixture should preferably be held below 350°C, at which the constituents decompose.

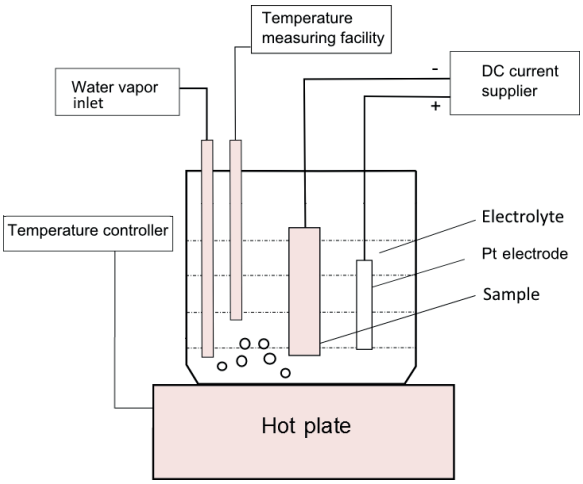

Figure. 1: Illustration of a cathodic hydrogen charging setup.

Criticism of the method has been raised, suggesting that the supersaturation of hydrogen causes high concentration gradients between the surface and interior [44], with a corresponding increase in stresses and structural damage in near surface regions, which could result in surface hardening of the charged material. The hardening is further believed to mask the studied hydrogen effect on the mechanical properties during a tensile test [15, 44]. Another commonly found dubiety regarding all the different charging methods is outgassing, in which the introduced hydrogen is believed to vaporize from the sample as soon as the charging procedure ends. For further details on the cathodic charging procedure used in this work, please *cf.* Paper I [45]. A summary of the charging results are presented in Section 6.

3.2 Hydrogen concentration profile

To calculate specific concentrations at various diffusion lengths using a solution to Fick's second law, the surface concentration of atomic hydrogen must be determined. If hydrogen gas charging methods are used, Sievert's law gives a good estimation [37]. However, for cathodic charging methods, the calculations are more complex. Any analytical solution regarding surface concentration of available hydrogen during a cathodic charging process is based on temperature, applied electric potential, proton conductivity of the electrolyte, and the electrochemical reaction. As with any charging method, the mechanism is also to some extent dependent on the surface chemistry and topology of the sample, as this may influence the dis-

sociation rate of molecular hydrogen into atomic hydrogen before entering the sample [46-48]. In addition, many of these factors may change during the charging process. The complexity of this evaluation and the difficulties of obtaining trustworthy results have been highlighted in a previous evaluation of the cathodic charging method [44].

3.2.1. Electromigration

To estimate the time, t, for hydrogen to reach the center of the sample, r_0, during cathodic charging, approximate calculations based on $\sqrt{2Dt} \geq r_0$ are commonly found in the literature. This estimation is based on a diffusion constant, D, in which only concentration driven diffusion is considered [3, 39, 43, 49]. This results in an overestimated charging time and underestimated diffusion length of hydrogen, which could lead to questionable conclusions regarding the hydrogen effect on the embrittlement mechanisms [50].

During cathodic charging, diffusion is not only driven by the concentration gradient but also by electromigration. This is caused by the applied electric potential. The potential drop in the length of the conducting sample rod is negligible, and its surface could be considered as an isopotential. The movement of the charge carriers close to the sample surface (*e.g.* migrating hydrogen ions), is assumed to follow the electric field in the electrolyte, which is approximately radial. The general time dependent diffusion equation (Fick's second law) reads

$$\frac{\partial C}{\partial t} = \nabla \cdot (D \nabla C) \tag{1}$$

where C is the concentration of the diffusing element and D the diffusion coefficient. The diffusion coefficient is defined as $D = D_0 \exp(-H_D/RT)$, where R and T are the gas constant and absolute temperature, respectively. An activation energy, H_D for hydrogen diffusion in IN718 of 48.63 kJ/mol was assumed [48]. The pre-factor D_0 has a reported range of 1.6-6.16×10-7 m^2/s and are based on results of hydrogen permeation tests on IN718 [48-50]. For our evaluation, we have chosen a value of $D_0 = 4.0 \times 10^{-7}$ m^2/s, which is close to the results from gas permeation test results and the value used in previous charging [3, 39]

When electromigration is considered, the diffusion coefficient is reportedly scaled by the electromigration factor ϕ [51], which is multiplied by the component of the charging current density vector $\mathbf{j}$ in the direction of the flux, and the sample radius, r_0. This anisotropic behavior of the diffusion coefficient is represented in the computation as a symmetric matrix in cylindrical coordinates with

$$D_r = D(1 + \phi j r_0) \tag{2}$$

and

$$D_z = D. \tag{3}$$

The electromigration factor is defined as

$$\phi = \frac{Z^* e \rho}{kT} \tag{4}$$

where Z^* is the effective charge number of the migrating particle. The resistivity, ρ, for IN718 at 300°C is measured to be around 1.32×10^{-6} Ωm [52]. Further, e is the electron charge with 1.602×10^{-19} C, and k is the Boltzmann constant.

Z^* is a dimensionless, experimentally determined parameter, which is a summation of the direct electrostatic force and the electron wind force. For H^+ the effective charge number in an NbV alloy was found to be close to unity, and not reported to be sensitive to temperature or to variations in alloy composition [53]. No value has to our knowledge been reported for H^+ in Ni-based alloys, but for pure Ni a value of 0.5 has been quoted, and investigations on various polycrystalline metals as well as several alloys, report values of 0.4-1.6 [54, 55]. In this work we will assume $Z^*= 1$.

4 Material model

In almost any application it is of great importance to know the yield stress and the continuous flow stress during the deformation process. In models on material deformation, the constitutive equations usually express these stresses as functions of other parameters, such as the plastic strain, the strain rate and the temperature. The models can be empirical or semi-empirical, and are commonly referred to as phenomenological material models. Two of the most used phenomenological models are the Johnson-Cook model and the Armstrong-Zerilli model [56]. These models are implemented in much finite element software such as ABAQUS [57] and MARC [58].

Another way to describe the material behaviour during plasticity is to use physically based material models. The advantage of physically based models is that they usually show deformation behaviour accurately for temperatures and strain rates well outside its fitting range. On the other hand they typically contain a large number of material parameters and could in some cases need a lot of experimental data. As the yield stress in a practical case is controlled by several different mechanisms, these have to be acknowledged and superimposed. Different mechanisms are usually dominant at different values of the state variables during deformation. This behavior can be visualised by the use of so-called deformation mechanism maps [59].

Additive assumption of different stress terms when modeling the yield stress is adopted by for example Nemat-Nasser *et al.* [60, 61] and Lindgren *et al.* [62]. The selected approach describes the yield stress with several different stress terms, usually with an athermal (σ_G) and a thermally activated (σ^*) term:

$$\sigma_y = \sigma_G + \sigma^* + \sigma_p + \ldots \tag{5}$$

The dots indicate that this can be extended with, or separated into, any physically motivated contributing stress term that is needed for describing the material of study, such σ_{HP} (Hall-Petch effect) or σ_{ss} (solid solution strengthening). In the present study of IN718, the hardening effect of precipitates is accounted for in a separate stress term, σ_p.

4.1 Long-range stress term

The athermal, or long-range term, which sometimes is referred to as the Taylor equation because of its origin [63], describes the long-range contribution to the yield stress caused by interactions between dislocations and lattice defects. The term is written as [64]:

$$\sigma_G = \alpha M G b \sqrt{\rho_i} \tag{6}$$

The only lattice defect representation in Eq. (6) is the density of immobile dislocations, ρ_i. For this reason the use of the contributing term should be restricted to coarse-grained, "structureless" materials [65] with fcc or close packed hexagonal crystal structures, where the lat-

tice resistance is negligibly small [66]. The Taylor orientation factor, M, converts the resolved shear stress for the slip systems of the crystal into equivalent effective stress. Although mentioned to be effected by texture, which evolves during plastic deformation, the Taylor factor is assumed to be constant and for fcc materials having a value of 3.06 [66, 69, 71]. The reason Eq. (6) sometimes is referred to as the athermal term is that thermal vibrations do not assist any moving dislocation in overcoming the obstacles described in the term. But the stress contribution in all is not temperature independent as both the shear modulus G and the proportionality factor α are temperature dependent at different degrees [67, 70]. Further, b is Burgers vector.

4.1.1. Dislocation density evolution

The density of mobile dislocations is assumed to be strain and stress independent and with a total density much smaller than that of immobile dislocations. Following the HELP description, dislocations could become mobile more easily under an increased hydrogen concentration. Even so, the total number of mobile dislocations during deformation is assumed to be constant. The density of immobile dislocations, used in Eq. (6), on the other hand evolves during plastic deformation. A general description of the evolution is based on the linear combination of two processes, storage and recovery [64, 67]. This can be expressed as:

$$\dot{\rho}_i = \dot{\rho}_i^{(+)} - \dot{\rho}_i^{(-)} \tag{7}$$

The storage, or hardening, is associated with an increase in the density of immobile dislocations. As the increase in immobile dislocations is physically related to the immobilization of mobile dislocations at obstacles that cannot be overcome, the evolution is described by the mean free path of the moving dislocations Λ and the structure parameters M and b [62, 64, 68]:

$$\dot{\rho}_i^{(+)} = \frac{M}{b}\frac{1}{\Lambda}\dot{\varepsilon} \tag{8}$$

The increment of this dislocation density $\dot{\rho}_i^{(+)}$ is expressed per increment in plastic strain $\dot{\varepsilon}$.

The mean free path is proportional to the characteristics of the microstructure, one of these being the grain size. The grain size dependence on the hardening of the material, the Hall-Petch effect, is accounted for via the grain size parameter g. Another parameter related to the microstructure characteristics is the diameter of the dislocation subcell s and is also represented in the expression for mean free path:

$$\frac{1}{\Lambda} = \left(\frac{1}{g} + \frac{1}{s} + \text{others}\right) \tag{9}$$

Depending on the material of study the term named *others* in Eq. (9) can incorporate other factors that alter the mean free path of mobile dislocations, such as precipitates. For the precipitation hardened alloy IN718, Fisk *et al*. [64] included the average distance between the precipitates l_p together with a proportionality factor, which only should be considered if this distance is shorter than the subcell diameter. It was concluded not to be the case for IN718 and the proportionality factor was set to zero. The parameter s is said to represent the dislocation substructure, by being the subcell diameter. Lindgren *et al.* [66] consider s representing the effect of all of the dislocation structures on the mean free path. They recognize the connection between s and the dislocation density as:

$$s = K_c \frac{1}{\sqrt{\rho_i}} + s_\infty \tag{10}$$

In Eq. (10) a lower limit for the subcell size s_∞ could be added. In the expression K_c is a proportionality factor concerning the subcell. The following expression for the increase of immobile dislocations with Eq. (10) and Eq. (9) is then:

$$\dot{\rho}_i^{(+)} = \frac{M}{b}\left(\frac{\sqrt{\rho_i}}{K_c} + \frac{1}{g}\right)\dot{\varepsilon} \tag{11}$$

The other part of the dislocation density evolution is the decrease of density, denoted $\dot{\rho}_i^{(-)}$ and referred to as the recovery term. This recovery or softening is believed to be controlled by two main mechanisms. One mechanism is the thermally activated and strain dependent dislocation glide or cross-slip, which leads to dislocation annihilation [64, 69]:

$$\dot{\rho}_{i1}^{(-)} = \Omega \rho_i \dot{\varepsilon} \tag{12}$$

Here Ω is a temperature dependent, but strain-independent material constant, commonly referred to as the recovery function [68, 70]. The strain rate factor limits this recovery mechanism to being purely dynamic. The other mechanism for recovery is dislocation climb which is defined as:

$$\dot{\rho}_{i2}^{(-)} = 2K_v D_s \frac{V_i}{V_0}\frac{Gb^3}{kT}(\rho_i^2 - \rho_{i0}^2) \tag{13}$$

The mechanism is strongly temperature dependent as being a function of the self-diffusion term D_s. Self-diffusion is assumed to predominantly being lattice localised. The vacancy concentrations are denoted V_i (instantaneous) and V_0 (initial), respectively. Vacancies in the lattice can be produced during cold working deformation. At higher temperatures it is assumed that the diffusivity of vacancies is high, leading to rapid annihilation. If the strain rate is high enough, the vacancy production increases and an excess is quickly reached. Models of this vacancy evolution have been proposed and could be attended if needed in the area of study

[76]. Because of the strong temperature dependence, the recovery mechanism of climb is believed to have little effect at temperatures at and below 400°C. This is why the calibration parameter K_v is both assumed [66] and optimised [67] to zero at these temperatures. Furthermore, k and T in Eq. (13) are the Boltzmann constant and absolute temperature respectively.

4.2 Short-range stress term

The second term in Eq. (5) has its foundation in Orowans work [71] on the role of discrete obstacles and their effect on the flow rate. The obstacles, which could be immobile dislocations, precipitates or solutes, serve as thermodynamic potential barriers that could be overcome by external stress and/or thermal vibration. The thermal activation follows an Arrhenius relation in the definition of plastic strain rate [61, 72]:

$$\dot{\varepsilon} = \dot{\varepsilon}_0 \exp\left(-\frac{\Delta G}{kT}\right) \tag{14}$$

The pre-exponential term, $\dot{\varepsilon}_0$, have been reported with a variation in the dependent parameters. But usually it is disclosed comprising the following [60, 61, 64]:

$$\dot{\varepsilon}_0 = b\rho_m l v_0 \tag{15}$$

Besides the density of mobile dislocations, ρ_m, the parameters are the average travel distance for a moving dislocation, l, and Burgers vector. The attempt frequency, v_0, is the vibration of the dislocation at an obstacle. Generally $\dot{\varepsilon}_0$ is considered a constant. The Gibbs free energy of activation for the moving dislocation to overcome any obstacle, either by bypassing or cutting, was derived by Kocks *et al*. [73] as:

$$\Delta G = \Delta F \left[1 - \left(\frac{\sigma^*}{\hat{\tau}}\right)^p\right]^q \tag{16}$$

This expression was a step forward in the description of the short-range obstacles when described as potential barriers. These where previously viewed as being uniformly spaced and box-shaped, but could now be shaped by the use of the exponents $0 \leq p \leq 1$ and $1 \leq q \leq 2$. The parameter $\hat{\tau}$ is the so called "athermal flow strength". It need to be exceeded in order to overcome obstacles in the absence of thermal energy. The value of $\hat{\tau}$ is proportional to the density and distribution of the obstacles in the glide plane as $\hat{\tau} \propto Gb/l$. Here l is said to be the obstacle spacing [63]. If, and only if an isotropic material, with equally-spaced obstacles can be assumed, this length is the same as the travel distance, or mean free path used in Eq. (8). Further, the athermal flow strength could also be related as being a function of an initial immobile dislocation density as $\hat{\tau} = Gb\sqrt{\rho_{i0}}$ [64].

The activation energy ΔF in Eq. (16) is the total free energy needed to move across the obstacles without any help from external stress and is dependent on the characteristics of the obstacles. It and can be quantified as $\Delta F = \Delta f_0 G b^3$. The coefficient is related to the obstacle

strength as shown in Table 1, which also displays the relation between obstacle spacing and the athermal flow strength.

Table 1: The influence of the obstacle characteristics on the activation energy and athermal flow strength [59].

Obstacle strength	Δf_0	$\hat{\tau}$	Example
Strong	2	$> \frac{b}{l}$	Dispersions: large or strong precipitates
Medium	$0.2 - 1.0$	$\approx \frac{b}{l}$	Small or weak precipitates
Weak	< 0.2	$<< \frac{b}{l}$	Lattice resistance; solution hardening

By combining of Eq. (14) and Eq. (16) an expression for the short-range stress contribution can be written as:

$$\sigma^* = \hat{\tau}\left(1 - \left(\frac{kT}{\Delta f_0 G b^3}\ln\left(\frac{\dot{\varepsilon}_0}{\dot{\varepsilon}}\right)\right)^{1/q}\right)^{1/p} \tag{17}$$

4.2.1. Solute concentration effect

Solid solutes are alloying elements not part of any precipitates within the host lattice. The solutes could either be interstitial solutes which at elevated temperatures could move more freely, or substitutional solutes with a movement dependent on lattice vacancies.

The general effect of solutes on the dislocation energy was described by Kocks [72] in the so-called *trough model*. In this description, dislocations interact with solutes that are recognised as discrete, but treated as being smeared out on the whole length of the dislocation line. Sometimes this is described as a solute atmosphere surrounding the dislocation core. This collective interaction could lower the dislocation line energy with a square-root relationship to the concentration of the solute creating a *trough* for the dislocation. In order to move on, the dislocation must leave this low energy bound state and obtain a free, high energy state, by nucleating a bulge. The lengths of the dislocation line and the bulge length are both important parameters in the description. It is also stated that some solutes very well could act repulsive and instead raise the dislocation line, or stacking fault, energy [60, 72].

Based on the foundation of the *trough model* together with reasoning around the alteration of the Peierls (lattice) potential because of the presence of solute atoms, Cheng *et al.* [60] extends the relationship of ΔF and $\hat{\tau}$ used in Eq. (16). The extension makes the relations dependent on the instantaneous dislocation localised solute concentration C as:

$$\Delta F = F_0' \sqrt{\frac{C}{C_0}} \tag{18}$$

and

$$\hat{\tau} = \tau_0 \sqrt{\frac{C}{C_0}} \left(\frac{l_0}{l_d} \right) \tag{19}$$

The initial, bulk concentration of the solutes are given by C_0. In Eq. (14) F_0' is the activation energy, at a dislocation solute concentration of C_0. The initial average dislocation link length is l_0, while the current dislocation link length is represented by l_d. Several descriptions report this length ratio depending on the accumulated strain and temperature, which has been proposed as an empirical model:

$$\frac{l_0}{l_d} = f(\varepsilon, T) \tag{20}$$

For constraining conditions as well as elaborations regarding the material parameters governing the function, please *cf.* [60, 74, 75].

The short-range stress term can be extended to accommodate a solute concentration of the bulk and at the dislocation core with the following expression:

$$\sigma^* = \tau_0 \sqrt{\frac{C}{C_0}} f(\varepsilon, T) \left(1 - \left(\frac{kT}{\Delta f_0 G b^3 \sqrt{\frac{C}{C_0}}} \ln \left(\frac{\dot{\varepsilon}_0}{\dot{\varepsilon}} \right) \right)^{1/q} \right)^{1/p} \tag{21}$$

The concentration of the solute at the dislocation core C will reach a saturation level as the solutes are diffusing under the influence of the dislocation stress field. The saturation level is dependent on available core sites for the solute, such as interstitial sites and vacancies. As the dislocation line bulges out under the applied stress, the dislocation core sweeps a new area with new core sites, why this concentration could vary dynamically [60]. This variation could manifest itself macroscopically as serrations in the stress-strain curve during tensile tests. In these cases the mechanism is usually called dynamic strain aging (DSA).

To accommodate the effect of individual core and bulk solutes on the short range term, it is proposed as [60, 62]:

$$\sigma^* = \tau_0 \sqrt{1 + \sum_i \frac{C^i - C_0^i}{C_0^i}} \left(1 - \left(\frac{kT}{\Delta f_0 G b^3 \sqrt{1 + \sum_i \frac{C^i - C_0^i}{C_0^i}}} \ln\left(\frac{\dot{\varepsilon}_0}{\dot{\varepsilon}}\right) \right)^{1/q} \right)^{1/p} \tag{22}$$

Solute concentration localised at the dislocation core is represented by C^i and should be equal or greater than the bulk concentration C_0^i. The concentrations have a dependence on, and is effectively a function of the plastic strain rate, as solutes diffuse towards the dislocation core, but also the temperature via the coefficient of solute lattice diffusion $D_l = D_0 \exp(-Q_l/kT)$ as:

$$\frac{C^i - C_0^i}{C_0^i} = \left(\frac{C_s^i}{C_0^i} - 1\right)\left(1 - \exp\left(-h \frac{D_l \dot{\varepsilon}_0}{b^2 v_0 \dot{\varepsilon}}\right)^{\xi}\right) \tag{23}$$

Further h is a proportionality factor and v_0 and b once again are the parameters attempt frequency and Burgers vector, respectively. In the case of lattice diffusion, ξ is 2/3. The concentration of solutes, including hydrogen, reaches a saturation level in the dislocation core, represented by C_s.

Hydrogen as solute

The previously mentioned solute atmosphere, when hydrogen is the solute, is commonly described as hydrogen residing in either normal interstitial lattice sites, or in trap sites. The trap sites for hydrogen could be reversible (mobile and immobile dislocations) or irreversible (second phase particles and interfaces and precipitates) [76, 77]. For the moving dislocation during plastic deformation, following the idea with the trough model description, the trap sites will mostly be reversible and these trap sites will effectively follow the moving dislocations carrying hydrogen. Furthermore, localization of hydrogen around the moving dislocation has been shown to follow the gradient of hydrostatic stress, why the concentration of hydrogen, as any other solute, is dynamic during deformation. If the only solute considered is hydrogen and in order to encompass the proposed HELP mechanism, where the yield stress is lowered in the presence of hydrogen, Eq. (22) is modified as:

$$\sigma^* = \tau_0 \frac{1}{\sqrt{1 + \frac{C - C_0}{C_0}}} \left(1 - \left(\frac{kT\sqrt{1 + \frac{C - C_0}{C_0}}}{\Delta f_0 G b^3} \ln\left(\frac{\dot{\varepsilon}_0}{\dot{\varepsilon}}\right) \right)^{1/q} \right)^{1/p} \tag{24}$$

As the stress term now encompasses the concentration of only hydrogen as solute, the effect of other solutes, if considered, should be represented by the previously mentioned additional stress term to Eq. (5) namely σ_{ss}.

4.3 Precipitate hardening contribution

Precipitates or obstacles and their effect on the flow stress could be incorporated in the short range term as described in Section 4.2. Although, for precipitation hardened alloys the effect could be described in a separate stress term in order to incorporate the size factor of the precipitates. The stress term σ_p in Eq. (5) represents this precipitation caused hardening. The term is a function of the material parameters M and b as well as the obstacle, or particle spacing, l_p as [78]:

$$\sigma_p = \frac{FM}{bl_p} \tag{25}$$

For small precipitates the moving dislocation will shear the particle into two parts during plastic deformation. This is generally not the case for larger precipitates. Rather, the moving dislocation will bow around. In the limit between the two phenomena, the particle has a size that is in its critical radius, r_c. For shearable particles, it is commonly assumed that the strength is linear dependent on the radius to the shear modulus and Burger's vector. For non-shearable particles, the obstacle strength is independent of the particle size, which gives the the following condition for the obstacle strength:

$$F = \begin{cases} 2\beta G b^2 \dfrac{r}{r_c}, & if\ r \leq r_c \\ 2\beta G b^2, & if\ r > r_c \end{cases} \tag{26}$$

where β is a fitting constant close to 0.5 [64].

4.4 Parameter values

Some of the parameter values of the stress term equations are based on previous work on IN718 [64] and fitted and refined based on tensile test results performed. The unknown parameters of Eq. (23) regarding the concentration change and saturation of hydrogen is determined by the use of a Matlab-based optimization platform together with tensile test results on both hydrogen charged and hydrogen free samples. Details on the determined parameters are disclosed in Paper III.

5 Inconel 718 - microstructure and composition

IN718 is a precipitation hardening alloy that contains four major phases, γ, γ', γ'' and δ together with varius types of carbides. It is primarily strengthened by the ordered body-centred-tetragonal (bct) compound, the γ''-phase. This disc-shaped precipitate can approximately be represented by Ni_3Nb. The face-centred-cubic (fcc) γ'-phase, $Ni_3(Al,Ti,Nb)$, also contributes to strengthening. Both γ' and γ'' phases commonly nucleates homogeneously within the fcc matrix, the γ-phase [2, 45, 87, 88]. The orthorhombic δ-phase usually nucleates at grain boundaries, but have also been observed to nucleate on stacking faults of γ''. The δ-phase show a similar composition as the γ'' but are more thermodynamically stable, why the growth of the δ-phase usually are on the expense of γ'' [87]. The precipitation of δ-phase usually requires an aging temperature above 850°C [79, 80].

Liu *et al.* concluded in their work that the precipitates in general, and the δ-phase specifically, increase the hydrogen susceptibility of IN718 [45, 89]. Tarzimoghadam *et al.* explains this δ-phase based enhanced susceptibility by a difference in solubility of hydrogen in the matrix and the δ-phase. The hydrogen could then get trapped in the interface and weaken the bond, with grain boundary decohesion as a resulting failure mechanism [81].

The material used in this work was delivered by Special Metals Wiggin Limited as cold drawn, precipitation hardened cylindrical IN718 rods, with chemical composition given in Table 2. As-recieved heat treatment procedures consisted of a solution treatment at 980°C for 1 h before water quenching. A subsequent precipitation heat treatment at 720°C for 8 h followed and ended with a cooling at 50°C/h to 620°C, and holding for 8 h.

Table 2: Chemical composition of the delivered IN718 (wt.%).

Ni	Cr	Fe	Nb	Mo	Ti	Al	Cu	Co	Mn	Si	C	P	S	B
53.38	18.57	Bal.	5.15	2.97	1.02	0.57	0.23	0.19	0.11	0.08	0.035	0.007	0.002	0.003

6 Summary of results

Presented in the section is a summary of the most relevant results. For a more detailed description and analysis, please *cf.* the appended papers. The summary focuses on the preparatory charging method and evaluation, as well as the experimental results. The initial succding parameter optimization for the proposed model is presented in Paper III, but this is an ongoing project which will be developed with extended experiments.

Computations

For an evaluation of the anisotropic diffusion process in an arbitrary cylindrical geometry, were both radial and longitudinal diffusion are considered, a finite volume PDE solver, FiPy, was used [82]. For evaluations on the corresponding geometry of the used tensile test samples, MARC [58] was used. The computations are based on solving Eq. (1) in two dimensions with radial and longitudinal diffusion coefficients of Eq. (2) and Eq. (3), respectively. This corresponds to an axisymmetric cylidrical grid. A small enough time step is chosen to assure stable solutions.

Table 3: Parameter values used in the computations.

Parameter	D_0 [m^2s^{-1}]	H_D [$Jmol^{-1}$]	R [$Jmol^{-1}K^{-1}$]	Z^* [-]	e [C]	ρ [Ωm]	k [JK^{-1}]
Used value	4.0×10^{-7}	48.63×10^{3}	8.314	1	1.602×10^{-19}	1.32×10^{-6}	1.38×10^{-23}

Computations of charging were done using an average current density of 0.6 mA/mm^2, a temperature of 250°C, sample radius of r_0 = 2.25 mm together with the electromigration parameter values given in Table 3. This yields a diffusion coefficient for radial diffusion (Eq. (2)) as almost 12 times larger than the diffusion coefficient for longitudinal diffusion, where electromigration is not considered (Eq. (3)).

$$D_r = D(1 + \phi j r_0) = 6.63 \times 10^{-11}\ \mathrm{m^2/s} \tag{27}$$

$$D_z = 5.56 \times 10^{-12}\ \mathrm{m^2/s} \tag{28}$$

Charging times where 25 h for the computation on the arbitrary volume, and both 25 h and 4 h for the computations representing a tensile test sample. Based on hydrogen concentration measurements of previously performed cathodic charging [45], a hydrogen concentration of 5 wt ppm (or about 300 at ppm) H is set as boundary conditions for the bottom end and outside surfaces. The top surface has a boundary condition of 0 wt ppm H. A reversed diffusion is computed for 1 year at room temperature, as a representation of a thought outgassing after the completed charging. For the reversed diffusion top, bottom and outside boundary conditions all have a concentration of 0 wt ppm H, while the initial condition inside the boundaries is set at 5 wt. This represents a homogeneously charged sample. Cross-section profiles of the computation results of the arbitrary volume can be seen in Fig. 2.

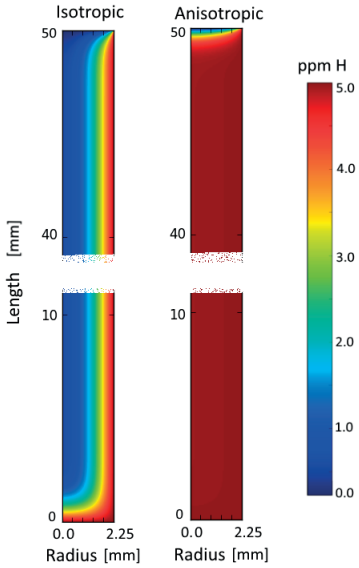

Figure 2: Comparative hydrogen concentration computation with either isotropic *D* (where all diffusion is only concentration driven) or anisotropic *D* (where the radial diffusion is both concentration and electromigration driven). Both cases are computed for a charging time of 25 h.

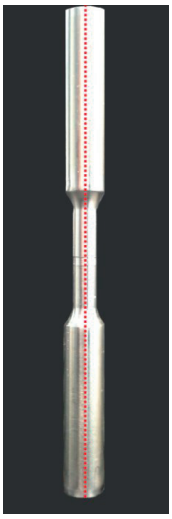

Figure 3: The symmetry axis of the tensile test sample used in the computations representing the tensile test sample.

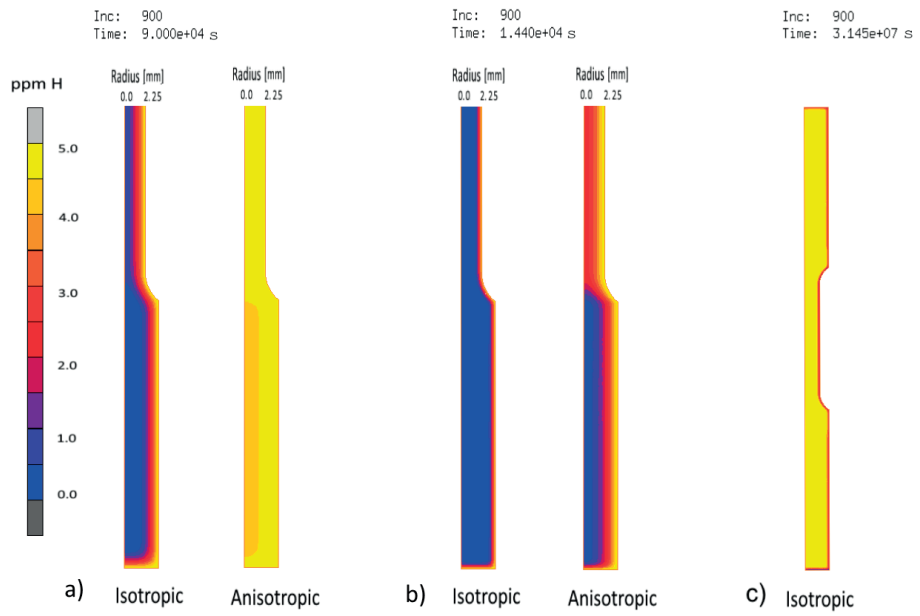

Figure 4: Comparative hydrogen concentration computation with either an isotropic *D* (where all diffusion is only concentration driven) or an anisotropic *D* (where the radial diffusion is both concentration and electromigration driven). The computations are performed for charging times of 25 h and 4 h in a) and b), respectively. A concentration gradient driven outgassing in room temperature is computed for 1 year with result shown in c).

The symmetry axis for the computations representing a tensile test sample is marked on the IN718 sample in Fig. 3. The resulting figures from the computation seen in Fig. 4, are reduced in length for more convenient display. The computations (Fig. 4a) show hydrogen concentration homogeneity for the 25 h charging, where anisotropic diffusion and electromigration is a factor. This homogenity is not seen in the isotropic case, where concentration driven diffusion is used in both the radial and the longitudinal direction. The computation for a 4 h charging time (Fig. 4b) reveals the evident effect electromigration has on the diffusion length of hydrogen into the sample. The level of outgassing at room temperature is show in Fig. 4c, and reveals a small surface localised outgassing. This is in good agreement with reported work [83] in which no significant outgassing of the previously introduced hydrogen could be detected for samples stored at room temperature for up to a year.

Hydrogen charging results

Hydrogen concentration measurements were performed by Swerea KIMAB, Sweden, using a LECO Rhen 602 thermal conductivity detection system. The method of measurement registers the full content of hydrogen within the sample, either if it is located at a trap site or a lattice site. The measured hydrogen concentration of cathodic charging performed at 250°C can be seen in Fig. 5. These samples were carefully lathed and then cut for radial concentration analysis. The result is normalised according to the depth gradient, which is believed to stem from an uneven distribution of hydrogen ions among the charge carriers in the electrolyte. This gives a clarified display of the hydrogen content at different radii of the sample. Measurements of the concentration for the reduced radius is in par with the previous shown computations, and do not provide support for any radial concentration gradient.

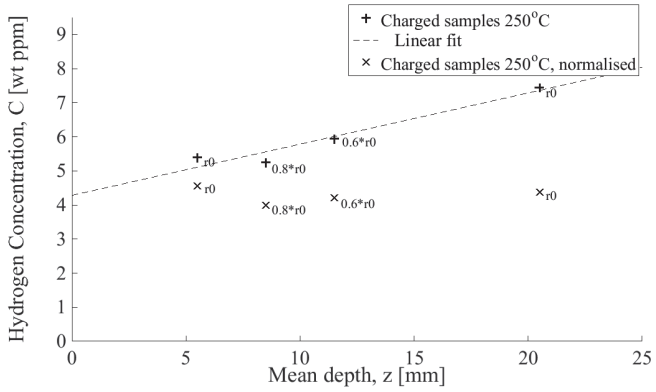

Figure 5: Measured hydrogen content of samples charged at 250°C, lathed down to different radii, where r_0 = 2.25 mm, and cut according to different depths into the electrolyte.

Surface imaging

Electron microscopy imaging of a sample charged at 250°C and an uncharged reference reveals changes in surface topology as a result of the charging[1]. Magnifications are 40x (Figure 2) and 1000x (Figure 3) Reviewing the images, the charging induced degradation seems to be surface localized with an effective depth of around 10 μm.

[1] The observed alteration of the surface topology is likely also responsible for alteration of the surface chemistry. This will to some degree change the rate of hydrogen uptake, but any further analysis regarding this change has not been undertaken.

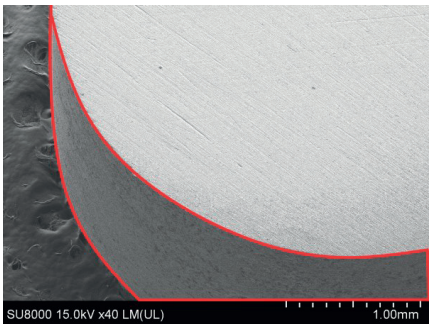

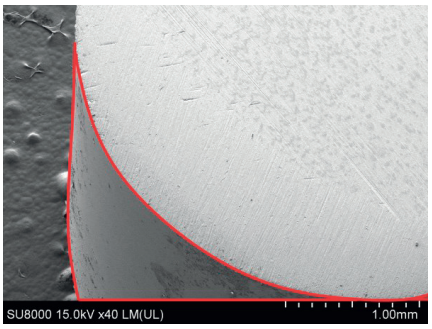

a) b)

Figure 2: SEM image of the exposed surface of the sample before and after charging, marked for clarification. Images recorded at 40x magnification.

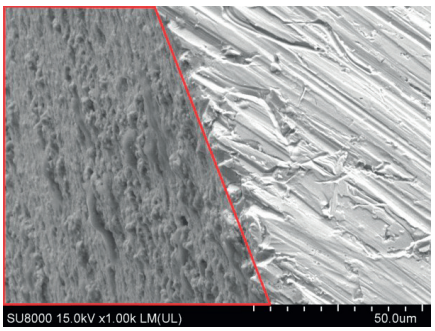

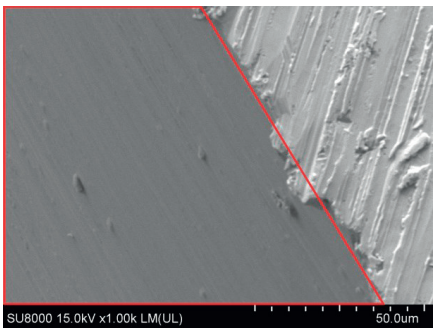

a) b)

Figure 3: SEM image of the exposed surface before and after charging, marked for clarification. Images recorded at 1000x magnification.

A clear difference can be seen in the macroscopic fracture of the tensile test samples. The uncharged sample in Fig. 6a bears trademarks of a ductile fracture, while the sample homogeneously charged with hydrogen in Fig. 6b, follow a brittle cleavage fracture. No microscopic analysis of the fracture surfaces where done at this point.

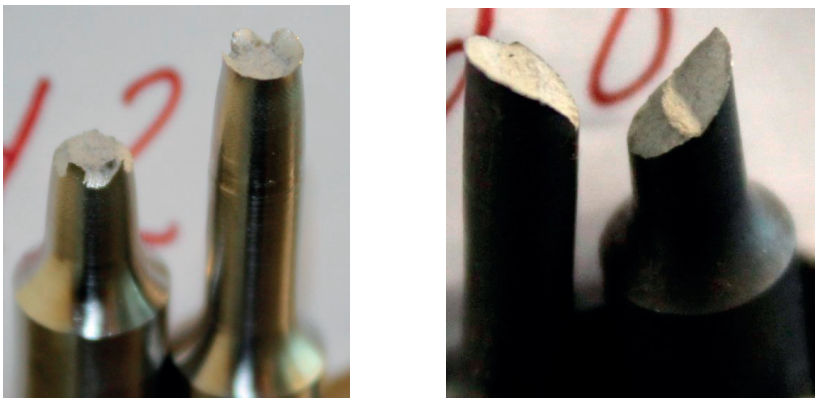

a) b)

Figure 6: The macroscopic difference in fracture apperance of (a) uncharged or (b) homogeneously charged samples of IN718.

Tensile test

Using an ASM tensile test machine, tensile tests were performed on both uncharged samples of IN718 and samples catholically charged using charging details to ensure hydrogen homogeneity. The strain rate used during the tests where 5.0×10^{-5} s^{-1}. The resulting stress strain curves are displayed in Fig. 7, in which a reduction in both yield and fracture strength can be seen in the charged samples, compared to the uncharged. Tensile test data are then used in a Matlab based material model optimisation platform, to extract the correct parameter values of the model described in Section 4.

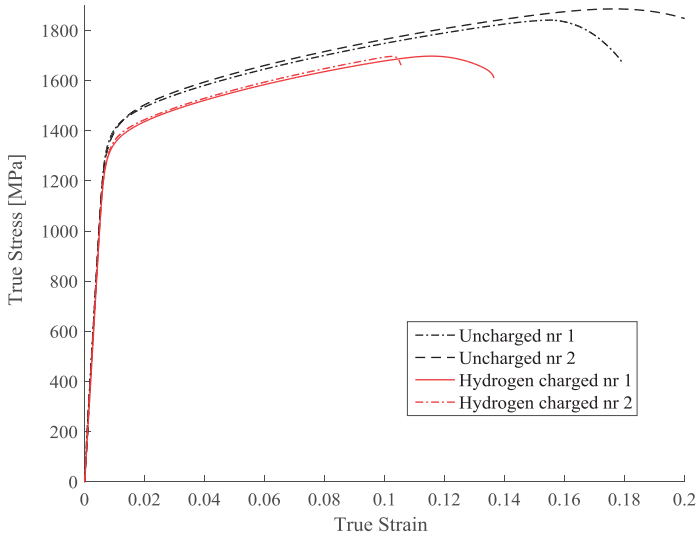

Figure 7: A comparative plot of the tensile test results of both uncharged and hydrogen charged IN718 samples.

7 Conclusions and further work

It has been shown that the driving force for hydrogen diffusion during cathodic charging cannot solely be explained by a concentration gradient, and that the applied electric potential must be accounted for. This is dealt with by implementing electromigration in the description of the diffusion process, which could be used to more accurately estimate the required charging time and minimize any unwanted side effects of the charging. Any validation of the electromigration parameters used in connection with the experimental results is beyond the scope of this study. Furthermore the outgassing of introduced hydrogen after completed charging is shown to be small in room temperature and should not be of any problem when the time between charging and tensile testing is reasonable.

The tensile tests result show characteristics which strenghtens HELP as the suggested mechanism of hydrogen induced failure in IN718. This includes a decrease in yield strength and premature failure, together with a macroscopic brittle fracture appearance.

An initial parameter study on the postulated material model, which includes the effect of hydrogen, has been initiated. The data is extracted from tensile tests performed on samples charged with hydrogen as well as uncharged reference samples of IN718. Complementary tensile tests on hydrogen charged IN718 samples will be performed, with varying strain rates. As the HELP mechanism and the “unlocking” of dislocations is dependent on the localisation of hydrogen and the hydrogen transport rate within the sample, there could be a strain rate limit in which the mechanism manifest itself.

Bibliography

[1] Slama C, Abdellaoui M. (2000) Structural characterization of the aged Inconel 718. *J Alloys Compounds* 306: 277-284.
[2] Reed RC. 2. The Physical Metallurgy of Nickel and its Alloys, *Superalloys - Fundamentals and Applications*: Cambridge University Press.
[3] Liu L, Tanaka K, Hirose A, et al. (2002) Effects of precipitation phases on the hydrogen embrittlement sensitivity of Inconel 718. *Science and Technology of Advanced Materials* 3: 335.
[4] Hirose A, Arita Y, Nakanishi Y, et al. (1996) Decrease in hydrogen embrittlement sensitivity of INCONEL 718 by laser surface softening. *Materials Science and Engineering: A* 219: 71-79.
[5] Sjöberg G, Cornu D. (2001) Hydrogen Embrittlement of Cast Alloy 718 - Effects of Homogenization, Grain Size and delta-phase: 679-690.
[6] Hicks PD, Altstetter CJ. (1992) Hydrogen-enhanced cracking of superalloys. *Metallurgical Transactions A* 23: 237-249.
[7] Hicks PD, Altstetter CJ. (1990) Internal hydrogen effects on tensile properties of Iron- and Nickel-base superalloys. *Metallurgical Transactions A* 21A: 365.
[8] Senor DJ, Peddicord KL, Strizak JP. (1991) Effects of hydrogen on the fracture morphology of Inconel 718. *Mater Lett* 11: 373-378.
[9] Robertson IM. (2001) The effect of hydrogen on dislocation dynamics. *Eng Fract Mech* 68: 671-692.
[10] Fritzemeier LC, Chandler WT. (1989) 15 - Hydrogen Embrittlement—Rocket Engine Applications, In: CAULFIELD, J.K.T. Ed, *Superalloys Supercomposites Superceramics*: Academic Press, 491-524.
[11] Nagumo M. (2004) Hydrogen related failure of steels - a new aspect. *Materials Science and Technology* 20: 940-950.
[12] Sirois E, Birnbaum HK. (1992) Effects of hydrogen and carbon on thermally activated deformation in nickel. *Acta Metallurgica et Materialia* 40: 1377-1385.
[13] McEvily AJ, Le May I. (1991) Hydrogen-assisted cracking. *Mater Charact* 26: 253-268.
[14] Tetelman AS, Robertson WD. (1963) Direct observation and analysis of crack propagation in iron-3% silicon single crystals. *Acta Metallurgica* 11: 415-426.
[15] Birnbaum HK, Sofronis P. (1994) Hydrogen-enhanced localized plasticity—a mechanism for hydrogen-related fracture. *Materials Science and Engineering: A* 176: 191-202.
[16] Sakintuna B, Lamari-Darkrim F, Hirscher M. (2007) Metal hydride materials for solid hydrogen storage: A review. *Int J Hydrogen Energy* 32: 1121-1140.
[17] von Pezold J, Lymperakis L, Neugebeauer J. (2011) Hydrogen-enhanced local plasticity at dilute bulk H concentrations: The role of H–H interactions and the formation of local hydrides. *Acta Materialia* 59: 2969-2980.
[18] Birnbaum HK. (1989) Mechanisms of hydrogen-related fracture of metals. *Office of Naval Research* USN 00014-83-K-0468.
[19] Takano N, Kaida S. (2012) Crack Initiation by Cathodic Hydrogen Charging in Nickel Single Crystal. *ISIJ Int* 52: 263-266.
[20] Lunarska-Borowiecka E, Fiore N. (1981) Hydride formation in a Ni-base superalloy. *Metallurgical Transactions A* 12: 101-107.
[21] Milella P. (2013) Hydrogen Embrittlement and Sensitization Cracking, *Fatigue and Corrosion in Metals*: Springer Milan, 689-729.
[22] Chen X, Foecke T, Lii M, et al. (1990) The role of stress state on hydrogen cracking in Fe-Si single crystals. *Eng Fract Mech* 35: 997-1017.

[23] Robertson IM, Sofronis P, Nagao A, et al. (2015) Hydrogen Embrittlement Understood. *Metallurgical and Materials Transactions A* 46: 2323-2341.
[24] Matsumoto R, Taketomi S, Matsumoto S, et al. (2009) Atomistic simulations of hydrogen embrittlement. *Int J Hydrogen Energy* 34: 9576-9584.
[25] Clum JA. (1975) The role of hydrogen in dislocation generation in iron alloys. *Scripta Metallurgica* 9: 51-58.
[26] Gibala R. (1970) Hydrogen-dislocation interaction in iron. *Scripta Metallurgica* 4: 77-80.
[27] Wilcox BA, Huggins RA. (1960) Effect of hydrogen on dislocation locking in niobium. *Journal of the Less Common Metals* 2: 292-303.
[28] Combette P, Renard M, Grilhe J. (1972) Internal friction in nickel containing hydrogen effect of relaxation and trapping of dislocations by hydrogen. *physica status solidi (a)* 11: 677-688.
[29] Matsui H, Kimura H, Moriya S. (1979) The effect of hydrogen on the mechanical properties of high purity iron I. Softening and hardening of high purity iron by hydrogen charging during tensile deformation. *Materials Science and Engineering* 40: 207-216.
[30] Matsui H, Kimura H, Kimura A. (1979) The effect of hydrogen on the mechanical properties of high purity iron III. The dependence of softening in specimen size and charging current density. *Materials Science and Engineering* 40: 227-234.
[31] Beachem CD. (1972) A new model for hydrogen-assisted cracking (hydrogen embrittlement□). *Metallurgical Transactions* 3: 441-455.
[32] Matsumoto T, Eastman J, Birnbaum HK. (1981) Direct observations of enhanced dislocation mobility due to hydrogen. *Scripta Metallurgica* 15: 1033-1037.
[33] Robertson IM, Birnbaum HK. (2005) Dislocation mobility and hydrogen-A brief review. *11th International Conference of Fracture*.
[34] Lynch SP. (1988) Environmentally assisted cracking: Overview of evidence for an adsorption-induced localised-slip process. *Acta Metallurgica* 36: 2639-2661.
[35] Sofronis P, Liang Y, Aravas N. (2001) Hydrogen induced shear localization of the plastic flow in metals and alloys. *European Journal of Mechanics - A/Solids* 20: 857-872.
[36] Shivanyuk VN, Foct J, Gavriljuk VG. (2001) Hydrogen-enhanced microplasticity of austenitic steels studied by means of internal friction. *Materials Science and Engineering: A* 300: 284-290.
[37] Oriani RA. (1993) The physical and metallurgical aspects of hydrogen in metals. *ICCF4 Fourth International Conference on Cold Fusion*.
[38] Au M. (2007) High temperature electrochemical charging of hydrogen and its application in hydrogen embrittlement research. *Materials Science and Engineering: A* 454–455: 564-569.
[39] Fournier L, Delafosse D, Magnin T. (1999) Cathodic hydrogen embrittlement in alloy 718. *Materials Science and Engineering: A* 269: 111-119.
[40] Beloglazov SM. (2003) Peculiarity of hydrogen distribution in steel by cathodic charging. *J Alloys Compounds* 356–357: 240-243.
[41] Kimura A, Birnbaum HK. (1987) The effects of cathodically charged hydrogen on the flow stress of nickel and nickel-carbon alloys. *Acta Metallurgica* 35: 1077-1088.
[42] Panagopoulos CN, Georgiou EP, Chaliampalias D. (2014) Cathodic hydrogen charging of zinc. *Corros Sci* 79: 16-20.
[43] Liu L, Zhai C, Lu C, et al. (2005) Study of the effect of delta phase on hydrogen embrittlement of Inconel 718 by notch tensile tests. *Corros Sci* 47: 355-367.
[44] Ulmer DG, Altstetter CJ. (1987) Hydrogen concentration gradients in cathodically charged austenitic stainless steel. *J Mater Res* 2: 305-312.
[45] Ehrlin N, Bjerkén C, Fisk M. (submitted 2016) Cathodic hydrogen charging of Inconel 718. *AIMS Materials Science*.
[46] G A, C B. (1998) Surfaces, Oxford Chemistry Primer 59 Eds., Oxford: Oxford University Press.

[47] Kupka M, Stępień K, Nowak K. (2014) Studies on hydrogen diffusivity in iron aluminides using the Devanathan–Stachurski method. *Journal of Physics and Chemistry of Solids* 75: 344-350.
[48] ASTM. (2011) Standard Practice for Evaluation of Hydrogen Uptake, Permeation, Transport in Metals by an Electrochemical Technique G148-97.
[49] Liu L, Tanaka K, Hirose A, et al. (2003) Experimental and numerical analyses of the mechanism for decreasing hydrogen-embrittlement sensitivity of aged Inconel 718 by laser surface annealing. *J Laser Appl* 15: 134-144.
[50] Delafosse D, Magnin T. (2001) Hydrogen induced plasticity in stress corrosion cracking of engineering systems. *Eng Fract Mech* 68: 693-729.
[51] Chao B, Chae S, Zhang X, et al. (2007) Investigation of diffusion and electromigration parameters for Cu–Sn intermetallic compounds in Pb-free solders using simulated annealing. *Acta Materialia* 55: 2805-2814.
[52] Basak D, Overfelt RA, Wang D. (2003) Measurement of Specific Heat Capacity and Electrical Resistivity of Industrial Alloys Using Pulse Heating Techniques. *Int J Thermophys* 24: 1721-1733.
[53] Brouwer RC, Griessen R. (1989) Electromigration of hydrogen in alloys: Evidence of unscreened proton behavior. *Phys Rev Lett* 62: 1760-1763.
[54] Ho PS, Watson TS. (1989) Electromigration in metals. *Reports on progress in physics* 52: 301-348.
[55] van Ek J, Lodder A. (1994) Electromigration of hydrogen in metals: Theory and experiment. *Defect and Diffusion Forum* 115-116: 1-38.
[56] Samantaray D, Mandal S, Borah U, et al. (2009) A thermo-viscoplastic constitutive model to predict elevated-temperature flow behaviour in a titanium-modified austenitic stainless steel. *Materials Science and Engineering: A* 526: 1.
[57] Scanscot Technology, SIMULIA Abaqus, 2016. Available from: https://scanscot.com/products/simulia/abaqus/.
[58] MCS Software - Marc, 2016. Available from: http://www.mscsoftware.com/product/marc.
[59] Frost HJ, Ashby MF. (1982) Deformation-Mechanism Maps, The Plasticity and Creep of Metals and Ceramics, Pergamon Press.
[60] Cheng J, Nemat-Nasser S, Guo W. (2001) A unified constitutive model for strain-rate and temperature dependent behavior of molybdenum. *Mech Mater* 33: 603-616.
[61] Nemat-Nasser S, Guo W. (2005) Thermomechanical response of HSLA-65 steel plates: experiments and modeling. *Mech Mater* 37: 379-405.
[62] Lindgren L, Domkin K, Hansson S. (2008) Dislocations, vacancies and solute diffusion in physical based plasticity model for AISI 316L. *Mech Mater* 40: 907-919.
[63] Taylor GI. (1934) The Mechanism of Plastic Deformation of Crystals. Part I. Theoretical. *Proceedings of the Royal Society of London A: Mathematical, Physical and Engineering Sciences* 145: 362-387.
[64] Fisk M, Ion JC, Lindgren L. (2014) Flow stress model for IN718 accounting for evolution of strengthening precipitates during thermal treatment. *Computational Materials Science* 82: 531-539.
[65] Estrin Y. (1998) Dislocation theory based constitutive modelling: foundations and applications. *J Mater Process Technol* 80–81: 33-39.
[66] Kocks UF, Mecking H. (2003) Physics and phenomenology of strain hardening: the FCC case. *Progress in Materials Science* 48: 171-273.
[67] Estrin Y. (1996) 2 - Dislocation-Density–Related Constitutive Modeling, In: Krausz, A.S., , Krausz, K. Eds, *Unified Constitutive Laws of Plastic Deformation*, San Diego: Academic Press, 69-106.
[68] Babu B, Lindgren L. (2013) Dislocation density based model for plastic deformation and globularization of Ti-6Al-4V. *Int J Plast* 50: 94-108.

[69] Nes E. (1997) Modelling of work hardening and stress saturation in FCC metals. *Progress in Materials Science* 41: 129-193.
[70] Bergström Y, Granbom Y, Sterkenburg D. (2010) A Dislocation-Based Theory for the Deformation Hardening Behavior of DP Steels: Impact of Martensite Content and Ferrite Grain Size. *Journal of Metallurgy* 2010: 16.
[71] Orowan E. (1940) Problems of plastic gliding. *Proceedings of the Physical Society* 52: 8.
[72] Kocks UF. (1985) Kinetics of solution hardening. *Metallurgical Transactions A* 16: 2109-2129.
[73] Kocks UF. (1975) Chapter 4. Thermal activation. *Progress in Materials Science* 19: 110-170.
[74] Nemat-Nasser S, Li Y. (1998) Flow stress of f.c.c. polycrystals with application to OFHC Cu. *Acta Materialia* 46: 565-577.
[75] Kuhlmann-Wilsdorf D. (1999) The theory of dislocation-based crystal plasticity. *Philos Mag A* 79: 955-1008.
[76] Dadfarnia M, Martin ML, Nagao A, et al. (2015) Modeling hydrogen transport by dislocations. *J Mech Phys Solids* 78: 511-525.
[77] Pound BG. (1990) Hydrogen trapping in precipitation-hardened alloys. *Acta Metallurgica et Materialia* 38: 2373-2381.
[78] Fisk M, Lundbäck A, Edberg J, et al. (Submitted 2016) Simulation of microstructural evolution during repair welding of an IN718 plate. *Finite Elements in Analysis and Design*.
[79] Burke MG, Miller MK. (1991) Precipitation in alloy 718: A combined AEM and APFIM investigation. *Superalloys 718, 625 and Various Derivatives*: 337-350.
[80] Zhang HY, Zhang SH, Cheng M. (2013) Precipitation Kinetics and Behavior of delta phase in Inconel 718 Alloy. *Advanced Materials Research* 652-654: 1128-1131.
[81] Tarzimoghadam Z, Rohwerder M, Merzlikin SV, et al. (2016) Multi-scale and spatially resolved hydrogen mapping in a Ni–Nb model alloy reveals the role of the δ phase in hydrogen embrittlement of alloy 718. *Acta Materialia* 109: 69-81.
[82] Guyer JE, Wheeler D, Warren JA. (2009) FiPy: Partial Differential Equations with Python. *Computing in Science and Engineering* 11: 6-15.
[83] Gray HR. (1974) Embrittlement of Nickel-, Cobalt-, and Ironbase Superalloys by Exposure to Hydrogen TND-7805.